VOL 4, NO.2 (2024) 123-150
https://jagst.utm.my

JAGST
Journal of Advanced Geospatial Science & Technology

Modelling XCO_2 for Peninsular Malaysia using Satellite Data and Atmospheric Parameters

Hwee San Lim*, Chong Keat Sim, Mohd Zubir Mat Jafri
School of Physics, Universiti Sains Malaysia, 11800 Pulau Pinang, Malaysia

*Corresponding author: hslim@usm.my

Abstract – This study aims to develop an algorithm for calculating the column-averaged dry air mole fraction of carbon dioxide (XCO_2) over peninsular Malaysia using statistical methods. Data from five atmospheric variables consisting of the aerosol asymmetry factor (AAF), aerosol optical thickness (AOT), temperature (temperature), water vapor (H_2O vapor) and aerosol single scattering albedo (SSA) were utilized to develop a predictive XCO_2 regression model using multiple linear regression (MLR) for examining the impacts of the atmospheric variables on the XCO_2. The predictive XCO_2 regression model highly correlates with atmospheric variables (R2 = 0.68 for Northeast Monsoon and R2 = 0.64 for Southwest Monsoon). The validation results show that XCO_2 yielded a strong R2 for the Northeast Monsoon and Southwest Monsoon seasons, i.e., 0.84 and 0.83, respectively. The proposed regression model exhibited excellent agreement under different monsoon seasons in Peninsular Malaysia.

Keywords *– Carbon dioxide (CO_2), GOSAT, multiple linear regressions (MLR)*

Article History: Received 7 July 2024, Accepted 10 August 2024, Published 31 August 2024

How to cite: Lim, H. S., Chong, K. S. and Mat Jafri, M. Z. (2024). Modelling XCO_2 for Peninsular Malaysia using Satellite Data and Atmospheric Parameters. Journal of Advanced Geospatial Science and Technology. 4(2), 123-150.

1.0 Introduction

Carbon dioxide (CO_2) is an inodorous and transparent gas naturally occurring in our atmosphere. CO_2 has been recognized as a primary anthropogenic greenhouse gas (GHG) and plays an important role in climate change due to an effective thermal infrared (TIR) radiation absorber. It contributes up to 70% of global warming (Peters et al., 2011; Olivier et al., 2012). The increased presence of GHGs in the atmosphere causes significant problems and threatens the livelihood of our society. These gases have been associated with climate change, which has influenced land and water resources and food and pasture availability and have caused the disappearance of plants and animal species and loss of habitat.

The global carbon cycle is interconnected between the atmosphere, pedosphere, biosphere, geosphere, and hydrosphere (Finlayson-Pitts and Pitts, 1999). Anthropogenic activities such as fossil combustion, land use change, cement production, biomass burning and deforestation have contributed to atmospheric CO_2 over the past two centuries and remain the second largest source after the Industrial Revolution (Solomon, 2007; American Meteorological Society, 2012; Houghton et al., 2012).

As reported by the Fifth Assessment Report of the Intergovernmental Panel on Climate Change (IPCC), "natural and anthropogenic substances and processes that alter the Earth's energy budget are the drivers of climate change" (IPCC, 2013). Earth's global temperature has increased by 0.8 degrees in the last century, with more than half of the increase occurring in the previous thirty years (Blunden and Arndt, 2012). Analysis has shown that there is a 95% probability that this warming is attributed to an enhanced greenhouse effect (Berger, 2000). In addition, a strong "greenhouse effect" has increased the global radiative forcing to 1.846 Wm-2 in 2012 (Butler and Montzka, 2013; Huang et al., 2015).

Over the past few decades, the atmospheric gas abundances have been measured using balloons, aircraft and sparsely distributed measurement sites. These observations have produced important insights into flux variability. However, they lack high spatial coverage in ground-based observations. Currently, CO_2 concentrations are mainly measured from ground-based observation platforms distributed in different areas of the world. Mauna Loa station, which is located on a high volcano in the Hawaii islands, began to collect atmospheric CO_2 concentration in 1957, and the annual average level of CO2 is continuing to increase and currently is at 414.72 ppm in 2013 (Tans and Keling, 2014; Lindsey, 2022). Different stations in the Northern Hemisphere reveal the growth

rates of background CO_2 have varied from 1–3 ppmv over the past decade (Tsutsumi et al., 2006; Artuso et al., 2009; Hofmann et al., 2009; Wang et al., 2010). However, insufficient knowledge of the sources and sinks of CO_2 leads to significant gaps and large uncertainties in future climate predictions for the reason that observation of CO_2 is limited by spatial and temporal coverages (Stephens et al., 2007; Marquis and Tans, 2008; Yoshida et al., 2011). Since these monitoring stations are located sparsely, it is impossible to acquire data through them (Khattak et al., 2014). In addition, surface networks are limited in representing complex atmospheric mixing in the mid to high troposphere, where the surface signal is diluted (Huntzinger et al., 2012).

Satellite data acquired through the application of remote sensing have good spatial and temporal resolutions devoted to observations for estimating atmospheric CO_2 concentration (Baker et al., 2010). The accuracy of satellite measurements makes remote sensing a practical tool for monitoring atmospheric CO_2 concentration at the regional level (Rayner and O'Brien, 2001; Houweling et al., 2004). CO_2 concentration data from satellite retrieval based on CO_2 absorption spectra provide a long-term observation at the regional or global scale. For instance, two satellites are specifically designed to measure the column-averaged dry air mole fraction of carbon dioxide (XCO_2). They are Japan's Greenhouse Gases Observing Satellite (GOSAT) and NASA's Orbiting Carbon Observatory-2 (OCO-2) (Yue et al., 2015). These observations could enable researchers to efficiently understand the dynamic processes that influence atmospheric CO_2 concentrations and their effects on regional or global climate change (Miller et al., 2007; Chevallier et al., 2007).

GHG concentrations could not be measured directly using remote sensing techniques before 2002 (Revadekar et al., 2016). Thus, many studies have used the retrieved GOSAT data as a valuable tool to provide new data on greenhouse gases and atmospheric variables. For example, GOSAT data help decrease the estimated flux errors in global atmospheric transport models for investigating CO_2 sources and sinks (Miyamoto et al., 2013). Consequently, a method for converting aircraft profile data to column-averaged data was proposed in their study. Their analysis suggested that the aircraft data uncertainties were sufficiently small and could be used for primary validation of satellite data. Furthermore, the combination of the Scanning Imaging Absorption Spectrometer for Atmospheric Chartography (SCIAMACHY) and GOSAT data revealed that the global spatial coverage of the CO_2 map improved significantly regarding global CO_2 distribution return. This study proved the effectiveness of the combination method for the generation of global-

scale XCO_2 maps with higher temporal and spatial sampling by jointly using the SCIAMACHY and GOSAT XCO_2 datasets (Wang et al., 2014).

Among the current satellites, the dataset of Level 2 (V02.xx) column-averaged dry air mole fractions of atmospheric CO_2 (XCO_2) derived from GOSAT observations showed an approximate two (2) ppm standard deviation as compared with ground-based observations and airborne measurement data (Yokota et al., 2009; NIES GOSAT Project, 2012). Although satellite observations have very good spatial distributions, the satellite retrievals of CO_2 are severely restricted due to some disturbance factors, such as the presence of clouds and orbit configurations, creating extensively high uncertainties relative to ground CO_2 observations. For instance, it has been pointed out that only about 10% of GOSAT data can be used to retrieve XCO_2 due to cloud contamination (Morino et al., 2010). Understanding the spatial variability of CO2 needs immediate and serious attention by all relevant authorities worldwide, as it is an essential element that affects the quality of life (Mahapatra, 2010; Wu et al., 2012; Azid et al., 2014). So, Malaysia is also not excluded in these respects. However, research on atmospheric CO_2 in Peninsular Malaysia is limited due to the lack of ground-station data. Thus, obtaining continuous CO_2 measurements over the study area is a challenging task. In addition, the climatology of Malaysia is dominated by the northeast monsoon (NEM) and southwest monsoon (SWM). These monsoons have primarily encompassed a year and will affect the climate and atmospheric parameters differently. Therefore, the MLR was used for a spatial estimation algorithm based on GOSAT's retrieved mid-tropospheric CO_2 and its association with the selected atmospheric variables over Peninsular Malaysia (Kim et al., 2020, 2022; Dimitriadou and Nikolakopoulos, 2022; Yuvaraj, 2020). The novel algorithm would allow researchers to investigate and analyze the effects of atmospheric variables on CO_2 using statistical methods. The GOSAT satellite data and AIRS instrument data validate the proposed algorithm.

2.0 Data and Methodology

2.1 Site Description

Peninsular Malaysia, also known as West Malaysia, is located south of Thailand, north of Singapore and east of the Indonesian island of Sumatra. The geographical extent of the study area is 1-7° N and 99-105° E (Figure 1), which covers an area of approximately 131,587 km^2.

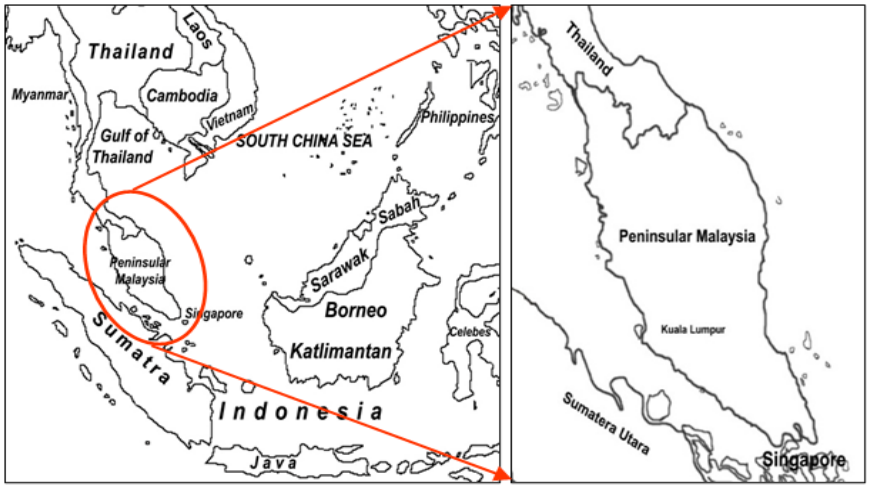

Figure 1. The geographical features of the study area.

Peninsular Malaysia is located near the equator and has a humid tropical climate; the weather is warm and humid throughout the year, with a temperature that varies between 20 °C and 32 °C (Omar, 2009). The local climate is affected by mountain ranges throughout Peninsular Malaysia; the climate can be divided into the highlands, the lowlands, and the coastal regions. The average monthly humidity falls between 70% and 90%, varying by location and month (Ahmad and Yassen, 2005). There is a definite variation in the monthly mean temperature that coincides with the monsoons, and there are annual fluctuations of approximately 1.5 °C to 2 °C.

There are two main monsoon regimes: the Northeast Monsoon (NEM), which occurs from November to March, and the Southwest Monsoon (SWM), which occurs from late May to September (Wong et al., 2009). The NEM originates from China and the northern Pacific, whereas the SWM originates from Australia's deserts. Furthermore, October is the transition month from the SWM to the NEM (Cruz et al., 2013). The maximum rainfall occurs in November for most areas in Peninsular Malaysia, and there is a second maximum rainfall during the inter-monsoon months of April or May. The lowest monthly rainfall occurs in February, and the highest in December (Varikoden et al., 2010). These monsoons are associated with many regional pollutant sources that affect atmospheric parameters and the amount of pollutants transported to Malaysia (Pochanart et al., 2003).

2.2 Instruments

GOSAT was successfully launched on January 23, 2009, from Tanegashima Island, Japan (JAXA, 2015). The average orbit altitude is 666 km; the local overpass time is 13:00, and there is a three-day repeat cycle (Kuze et al., 2009). The Thermal and Near Infrared Sensor for Carbon Observation (TANSO) onboard GOSAT has two optical units: the Fourier Transform Spectrometer (FTS) and the Cloud and Aerosol Imager (CAI). The TANSO-FTS instantaneous field of view (IFOV) is 15.8 mrad, corresponding to a nadir footprint diameter of approximately 10.5 km (Reuter et al., 2010; Bril et al., 2012). More details on the TANSO-FTS can be found in Kuze et al. (2009).

GOSAT data have been validated and consistently compared with other satellite aircraft and in situ data. The retrieval of XCO_2 from TCCON data represents a primary validation source for most of the satellite observations (Chahine et al., 2005, 2008; Kulawik et al., 2010; Crevoisier et al., 2009; Crisp et al., 2004; Bösch et al., 2006; Tahara and Usami, 2009; Yokomizo, 2008; Yokota et al., 2009). The Total Carbon Column Observing Network (TCCON) is a global ground-based Fourier Transform Spectrometer (FTS) recording direct solar spectra in the near-infrared spectral region. The column-averaged abundances of CO_2, CH_4, N_2O, HF, CO, H_2O, and HDO are retrieved from these spectra by the least-squares spectral matching algorithm. TCCON spectra have minimal influences from aerosol particles, air mass uncertainties, or variations in land surface properties (Wunch et al., 2011). Thus, TCCON data serve as a transfer standard between satellite observations and in situ networks (Reuter et al., 2011; Wunch et al., 2009, 2010, 2011; Yang et al., 2002). In addition, theoretical analyses have revealed that combining satellite measurements and inverse modelling can significantly diminish surface flux uncertainties. Sensitivity to all altitude levels containing the boundary layer should be possible using reflected solar radiation in the NIR or SWIR spectral region (Chevallier et al., 2007; Hungershoefer et al., 2010; Schneising et al., 2013).

The Atmospheric Infrared Sounder (AIRS) is one of several instruments onboard the Earth Observing System (EOS) Aqua satellite, launched on 4 May 2002. The Aqua satellite is in polar sun-synchronous orbit, flying at an altitude of approximately 705 km and completing an orbital cycle in 98.8 minutes. The platform's equatorial crossing is at 13:30 local time; the cycle period is 16 days (Aumann et al., 2003). The Aqua satellite includes two companion microwave instruments, i.e., the Advanced Microwave Sounding Unit (AMSU) and the Humidity Sounder for Brazil (HSB). The AIRS/AMSU/HSB combination provides coincident observations of the Earth's

atmospheric, land and ocean surface temperatures and greenhouse gases for analyzing several interdisciplinary issues in the earth sciences. The AIRS instrument offers new insights into weather and climate for the 21st century, obtains information regarding several GHGs (CO_2, CH_4, and CO), and studies the water and energy cycles (Haskins and Kaplan, 1992; Marshall et al., 2006). Previous studies showed CO_2 retrievals for clear-sky regions, which used measurements in limited time intervals, revealed the feasibility of obtaining successful CO_2 data sets and overcoming some outstanding problems (Chédin et al., 2003; Crevoisier et al., 2004; Tiwari et al., 2014). On the other hand, validation by comparison to in situ aircraft measurements and retrievals by land-based upward-looking Fourier Transform Interferometers proves that AIRS CO_2 is accurate to 1-2 ppm (Chahine et al., 2005, 2008).

2.3 Method of Analysis

The study primarily aimed to develop a predictive XCO_2 regression model over Peninsular Malaysia with data on atmospheric variables (AAF, AOT, temperature, H_2O vapor and SSA) as predictor variables based on the available data. This research used four years of data, encompassing April 2009 to December 2013, based on the available data in the study area. The related data was partly used to predict the regression model (2009-2012), and the final year, i.e., 2013, was used to validate and compare the regression model. The retrieved atmospheric standard products from the TANSO FTS SWIR Level 2 Version 02.28(v) and 02.29(v) data were downloaded from the GOSAT User Interface Gateway (GUIG) website (JAXA, 2015). The standard product used in this study is point data; the data footprint has a diameter of 10.5 km. The data for each variable were stored in HDF-EOS4 files, a convenient file extension. The data for each variable were extracted using HDFView and arranged into a table in MS Excel. The correlations between atmospheric parameters (AAF, AOT, temperature, H_2O vapor and SSA) and predicted XCO_2 equations were examined statistically using MLR by Statistical Package for Social Sciences (SPSS) software (Keat et al., 2014).

Regression analysis, or curve fitting, is a virtuous method for predicting outcomes from measured values of an explanatory variable within a specific probability range. Before interpreting the result, several fundamental assumptions of MLR were checked. An inspection of the standard probability plot of regression standardized residuals revealed that all the observed values fall roughly along the straight line, indicating that the residuals are from the normally distributed

population. An MLR equation was generated to estimate XCO_2 in peninsular Malaysia based on the individual *B* values:

$$Y_i = B_0 + B_1X_{1i} + B_2X_{2\,i} + B_3X_{3\,i} + B_4X_{4i\,....} + \beta_i \quad (1)$$

where *Y* is the response variable, $X_1, X_2, X_3 \ldots$ are observed values of $X_{1i}, X_{2i}, X_{3i} \ldots X_{qi}$ *for* $i = 1 \ldots n$ explanatory variable, B_0 is the regression equation constant, and $B_1, B_2, B_3, B_4 \ldots$ are the explanatory variable constants. Additionally, regarding β, multiple regression can help investigate the impact of several response variables ($X_{1i}, X_{2i}, X_{3i} \ldots$) to one explanatory variable (*Y*).

The temporal resolution of the AIRS Level 3 Standard products is daily, every eight days and monthly. The AIRS website provides all of the data, so we can access the AIRS website to acquire Level 3 data products quickly and easily. In this study, we used monthly ascending AIRX3C2M Level 3 data. The spatial resolution of AIRX3C2M is 2.5 degrees and 2.0 degrees in latitude and longitude. This monthly CO_2 standard products from AIRS Level 3 Version 5.9.14.0 were acquired for 2013. The AIRS data were employed to validate the predictive algorithm for XCO_2 in the NEM season and XCO_2 in the SWM season from GOSAT data. The data provide a clear interpretation of this study. AIRS data to validate XCO2 from GOSAT, despite AIRS having a coarser resolution, lies in its complementary strengths and the purpose of the validation. AIRS data, although coarser, provide valuable independent observations that can help confirm the accuracy and reliability of GOSAT measurements.

3.0 Results and Discussion

3.1 Generating Algorithm XCO_2 with GOSAT Data

As explained in Section 2.3, the MLR method was used to develop the predictive algorithms of XCO_2 over peninsular Malaysia based on the GOSAT data from 2009 to 2012. Data for five atmospheric variables (AAF, AOT, temperature, H_2O vapor and SSA) were used to generate the equation. Eq. (2) shows that the regression in terms of B was used to predict the XCO_2 for the desired study area. The equation is given as follows:

$$XCO_2 = B_0 + B_1AAF + B_2AOT + B_3Temperature + B_4H_2O\ vapor + B_5SSA \quad (2)$$

B_0 is the Regression Equation Constant, and B_{AAF}, B_{AOT}, $B_{Temperature}$, $B_{H2O\ Vapor}$, and B_{SSA} are the explanatory coefficients, respectively. Based on the data availability, 184 daily sampling points from Peninsular Malaysia were chosen to develop a predictive XCO2 regression model in different monsoon seasons (i.e., NEM and SWM). The number of sampling points for NEM and SWM were 84 and 100, respectively. The regression equations were determined to be:

$$XCO_2 = 607.95 + (-41.73)\ AAF + (-7971)\ AOT + (-0.6729)\ Temperature + (-2.05 \times 10^{-4})\ H_2O\ vapor + (44.31)\ SSA \quad (3)$$

$$XCO_2 = 591.18 + (-14.39)\ AAF + (-5619)\ AOT + (-0.6339)\ Temperature + (-3.56 \times 10^{-4})\ H_2O\ vapor + (26.15)\ SSA \quad (4)$$

for the NEM and SWM seasons, respectively.

The coefficients of determination (i.e., R^2) were 0.68 and 0.64 for the NEM and SWM seasons, respectively. Furthermore, the regression coefficients were statistically significant, and the ρ value of all the coefficients was less than 0.05 ($\rho < 0.05$). In statistical analysis, SPSS software generates the appropriate statistical analysis, the ρ-value associated with the test statistic, and a confidence interval for the mean difference over an independent samples t-test. Good agreement was found between the atmospheric variables and XCO_2 during the observation periods. The β coefficient was used in multiple regression analysis to study the impacts of AAF, AOT, temperature, H_2O vapor and SSA with XCO_2. Table 1 shows all the multiple regression results for NEM and SWM seasons regarding β.

Table 1. Estimated regression coefficient β 'standardized beta coefficient', for GOSAT data.

Atmospheric variables	Standardized beta coefficient, β	P-value	t-statistic
(a) NEM			
AAF	-0.38	0.00	-3.49
AOT	-0.61	0.00	-7.83
Temperature	-0.36	0.00	-3.70
H_2O vapor	-0.24	0.02	-2.46
SSA	0.31	0.00	3.28
(b) SWM			
AAF	-0.34	0.00	-1.40
AOT	-0.52	0.00	-8.5
Temperature	-0.33	0.00	-5.14
H_2O vapor	-0.10	0.03	-4.76
SSA	0.18	0.00	2.92

XCO_2 in peninsular Malaysia during the NEM season was most affected by AOT based on its highly negative β value. The highest negative β between AOT and XCO_2 was -0.610, statistically significant at a 95% confidence level. During this period, the volume size distribution was higher due to the hygroscopic growth of urban aerosol particles; the effect is nearly comparable to the 1% or four (4) ppmv change in the CO_2 concentration near the Earth's surface. This effect is caused by strong pulses of wind, commonly known as cold surge outbreaks from Siberia and Northeast Asia, that transport pollution over Southeast Asia due to the interaction with the heavily polluted regions of East Asia (Pochanart et al., 2003). The air pollutant levels in continental Southeast Asia increase simultaneously (Pochanart et al., 2005). During the SWM season, XCO_2 in Peninsular Malaysia was most affected by the AOT, indicated by the significant negative β value (-0.515) and statistical significance at the 0.05 level. Increased AOTs are mainly caused by biomass-burning activities and meteorological conditions during this season, such as relative humidity, temperature, and pressure. This relationship results from biomass burning activities and meteorological conditions, such as relative humidity, temperature and pressure (Dubovik et al., 2002). In addition, the impact of small to moderate amounts of air pollution transported by marine air masses from the Indian Ocean in the Southern Hemisphere to continental Southeast Asia enhances the atmospheric CO_2 concentration (Pochanart et al., 2003).

Principle component regression was used to compute the column-averaged dry air mole fraction of carbon dioxide (XCO_2) with five atmospheric variables (AAF, AOT, Temperature, H_2O vapor and SSA) over peninsular Malaysia. Table 2 shows the Pearson correlation matrices of the variables for NEM and SWM seasons.

Table 2. Pearson correlation matrix of different variables for NEM and SWM season. The statistically significant correlation coefficients ($\rho < 0.05$) are bolded.

	AAF	**AOT**	**Temperature**	**H_2O vapor**	**SSA**	**XCO_2**
(a) NEM season						
AAF	1	0.26	**-0.60**	**0.62**	**0.54**	**-0.31**
AOT		1	0.07	0.28	0.28	**-0.67**
Temp			1	**-0.50**	**-0.51**	0.13
H_2O vapor				1	0.24	**0.40**
SSA					1	0.06
XCO_2						1
(b) SWM season						
AAF	1	**0.33**	**-0.30**	**0.59**	**0.32**	**-0.32**
AOT		1	0.09	0.24	0.03	**-0.60**
Temp			1	**-0.33**	**-0.36**	**0.30**
H_2O vapor				1	0.10	**-0.40**
SSA					1	0.22
XCO_2						1

During the NEM season, XCO_2 was highly and negatively correlated with the AOT (-0.665) and moderately correlated with the AAF (-0.309), whereas XCO_2 was positively correlated with the H_2O vapour (0.393), temperature (0.127) and SSA (0.057). The increase in XCO_2 is associated with increased H_2O vapor, temperature and SSA and decreased AOT and AAF. These results were expected because these pollutants are known precursors of XCO_2. In the SWM season, XCO_2 was negatively correlated with the AOT (-0.656), H_2O vapor (-0.399), and AAF (-0.315) and positively correlated with the temperature (0.299) and SSA (0.219).

The PCA algorithm is beneficial in reducing data dimensionality by extracting the related variables and achieving better results. The first processing step was transforming the predictor variables into equal principal components. The primary objective was to get a small number of components that could elucidate most (60–90%) of the total variation in the predictor variables.

Next, varimax rotation was utilized to maximize the loading of a predictor variable on one component of PCA. Generally, applications of PCA procedures followed by a varimax rotation generate a ranked series of factors. Table 3 and Table 4 present the varimax rotation results of the five principal components, together with the amount of variance accounted for by each component for the NEM and SWM seasons, respectively.

Table 3. Rotated principal components loadings for NEM season.

Atmospheric variables	**PC1**	**PC2**	**PC3**	**PC4**	**PC5**
AAF	**0.82**	0.31	0.32	0.30	0.83
AOT	**0.83**	0.14	0.09	0.15	0.06
Temperature	0.13	**0.88**	-0.25	-0.29	-0.24
H_2O vapor	0.64	0.44	0.91	0.07	0.25
SSA	**0.75**	-0.01	0.07	0.94	0.21
Eigenvalue	2.76	1.59	0.81	0.40	0.29
% of Variance	45.99	26.47	13.56	6.68	4.76
Cumulative %	45.99	72.46	86.02	92.7	97.46

Table 4. Rotated principal components loadings for SWM season.

Atmospheric variables	**PC1**	**PC2**	**PC3**	**PC4**	**PC5**
AAF	**0.61**	0.60	0.17	0.29	0.91
AOT	**0.80**	-0.10	0.03	0.08	0.14
Temperature	0.11	**0.82**	-0.17	-0.16	-0.13
H_2O vapor	**0.63**	0.49	0.02	0.92	0.28
SSA	-0.08	0.70	0.97	0.02	0.14
Eigenvalue	2.29	1.78	0.82	0.53	0.37
% of Variance	38.23	29.61	13.66	8.87	6.09
Cumulative %	38.23	67.84	81.50	90.37	96.46

According to the Kaiser and Guttman rule, eigenvalues greater than or equal to 1 can be considered statistically significant. Tables 5 and 6 show that the first two principal components

(i.e., PC1 and PC2) were retained because they accounted for 72% and 67% of the total variation during the NEM and SWM seasons, respectively. For the NEM season, PC1 accounted for 46% of the total variation in the data, which was found to be loaded heavily on [AAF], [AOT], and [SSA], with small contributions from [temperature], and [H_2O vapor]. PC2, which accounted for approximately 26% of the total variation, was loaded heavily on [AOT], with only small contributions from [H_2O vapor] and [AAF]. Principal components three, four and five were loaded heavily on [H_2O vapor], [SSA] and [AAF], respectively.

Table 5. Rotated principal components loadings for NEM season.

Atmospheric variables	**PC1**	**PC2**	**PC3**	**PC4**	**PC5**
AAF	**0.82**	0.31	0.32	0.30	0.83
AOT	**0.83**	0.14	0.09	0.15	0.06
Temperature	0.13	**0.88**	-0.25	-0.25	-0.24
H_2O vapor	0.64	0.44	0.91	0.07	0.25
SSA	**0.75**	-0.01	0.07	0.94	0.21
Eigen value	2.76	1.59	0.81	0.40	0.29
% of Variance	45.99	26.47	13.56	6.68	4.76
Cumulative %	45.99	72.46	86.02	92.70	97.46

Table 6. Rotated principal components loadings for SWM season.

Atmospheric variables	**PC1**	**PC2**	**PC3**	**PC4**	**PC5**
AAF	**0.61**	0.60	0.17	0.29	0.91
AOT	**0.80**	-0.10	0.03	0.081	0.14
Temperature	0.11	**0.82**	-0.17	-0.16	-0.13
H_2O vapor	**0.63**	0.49	0.02	0.92	0.28
SSA	-0.08	0.70	0.97	0.02	0.14
Eigen value	2.30	1.78	0.82	0.53	0.37
% of Variance	38.23	29.61	13.66	8.87	6.09
Cumulative %	38.23	67.84	81.50	90.37	96.46

The pattern for the SWM season differed slightly from the NEM season for the first two principal components shown in Table 5. The remaining principal components accounted for progressively less of the total variation. Stepwise regression analysis was used to determine the original independent variables that are significant to the variation of the transformed XCO_2 observations based on the principal components selected as independent variables. The results of the analysis are summarized in Table 7.

Table 7. A linear regression model is used to predict XCO_2 using the principal components.

Predictors	Constant	PC1	PC2
(a) NEM season			
Adjusted R-squared		0.68	0.90
Estimated regression coefficient	391.39	0.83	0.95
(b) SWM season			
Adjusted R-squared		0.78	0.87
Estimated regression coefficient	390.17	0.87	0.93

The primary objective of the last section was to select a subset of predictor variables that produce the best predictive algorithm for XCO_2 based on the multiple linear regression method. The selected original independent variables were those with high loadings associated with each of the principal components included in the regression equation that had high coefficients of determination. Table 5 to Table 6 were used for the NEM and SWM seasons to match a PC in the regression analysis to an independent variable. In this study, only the highest loading for each PC was chosen for the XCO_2 prediction model because it produces an acceptable accuracy. Procedures for applying the highest loading used can be found in other studies (Abdul-Wahaba et al., 2005; Al-Alawi et al., 2008; Rajab et al., 2013). [AOT] was selected from PC1, and [temperature] from PC2. These two variables were then used as predictor variables in a subsequent regression analysis. The following regression models were derived:

For the NEM season:

(PCA1) XCO2 = 391.39 + 0.778 [AOT] + 2.530 [Temperature] (5)

For the SWM season:

(PCA2) XCO2 = 390.17 + 0.823 [AOT] + 2.488 [Temperature (6)

3.2 Validation of the Predicted XCO_2 with the Observed AIRS XCO_2

All prediction algorithms, i.e., XCO_2 in the NEM season and XCO_2 in the SWM season, were validated using independent observed GOSAT and AIRS data. The average relative difference between XCO_2 concentrations retrieved from observed GOSAT and AIRS was computed through GOSAT-retrieved XCO_2 datasets and AIRS-retrieved XCO_2 datasets. The mean relative difference for the XCO_2 data retrieved from GOSAT and AIRS is approximately 6%. Even though the mean relative difference exists between GOSAT-retrieved and AIRS-retrieved datasets, the relative difference remained within an acceptable range. The validations were conducted using the MLR method for both NEM and SWM seasons in 2013. First, the predicted XCO_2 values were validated against the observed XCO_2 values from the AIRS, and the coefficients of determination (R2) were analyzed. Figure 2 and Figure 3 shows the validation results for the predicted XCO_2 in the NEM and the SWM seasons, respectively; the predicted values are linearly and positively correlated with the observed XCO_2 values from the AIRS data. The R^2 were 0.80 and 0.80, respectively. The results show that the predicted XCO_2 and the observed XCO_2 from the AIRS instrument are highly correlated. These results indicate that the predicted XCO_2 is nearly identical to the observed XCO_2. Then, two predicted XCO_2 algorithms expressed in Eq. (3) and Eq. (4) were validated against observed XCO_2 obtained from GOSAT. The validation was performed from the NEM and SWM seasons in 2013, respectively.

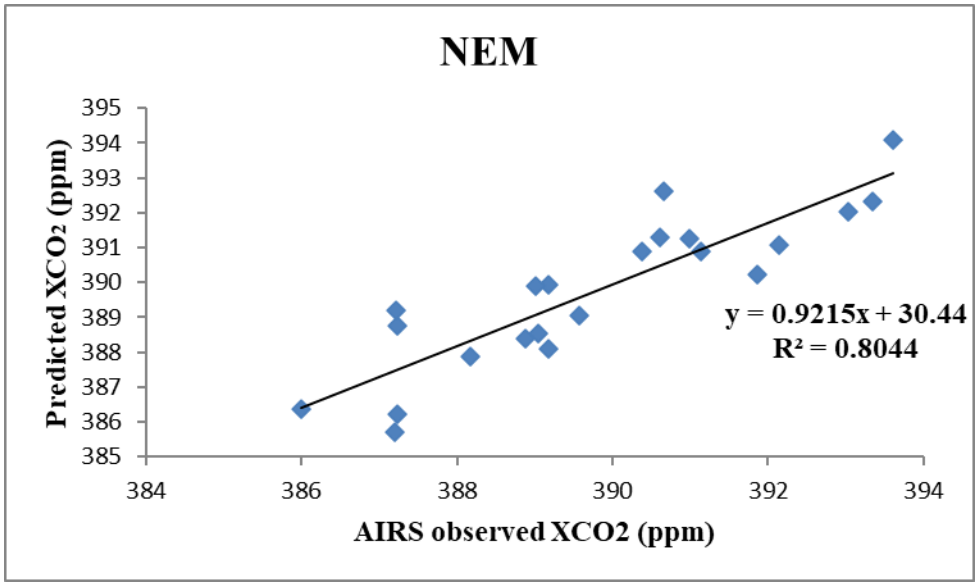

Figure 2. Predicted XCO_2 vs. observed XCO_2 from the AIRS for the NEM season.

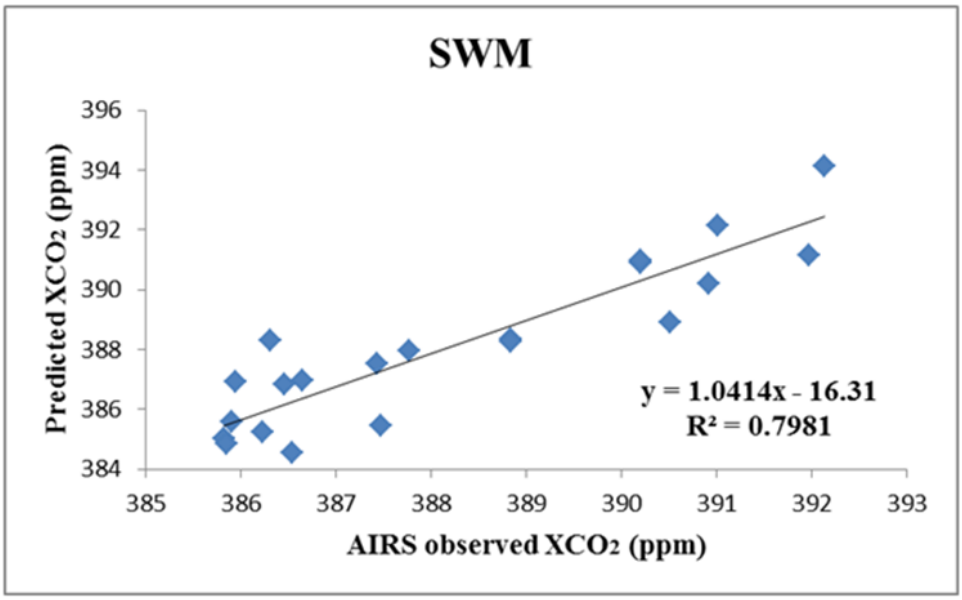

Figure 3. Predicted XCO_2 vs. observed XCO_2 from the AIRS for the SWM season.

Figure 4 and Figure 5 shows the validation results for the predicted XCO2 compared with the observed values from GOSAT. The predicted regression model of XCO2 yielded a strong R2 of 0.8412 and 0.8348 for the NEM and SWM seasons, respectively.

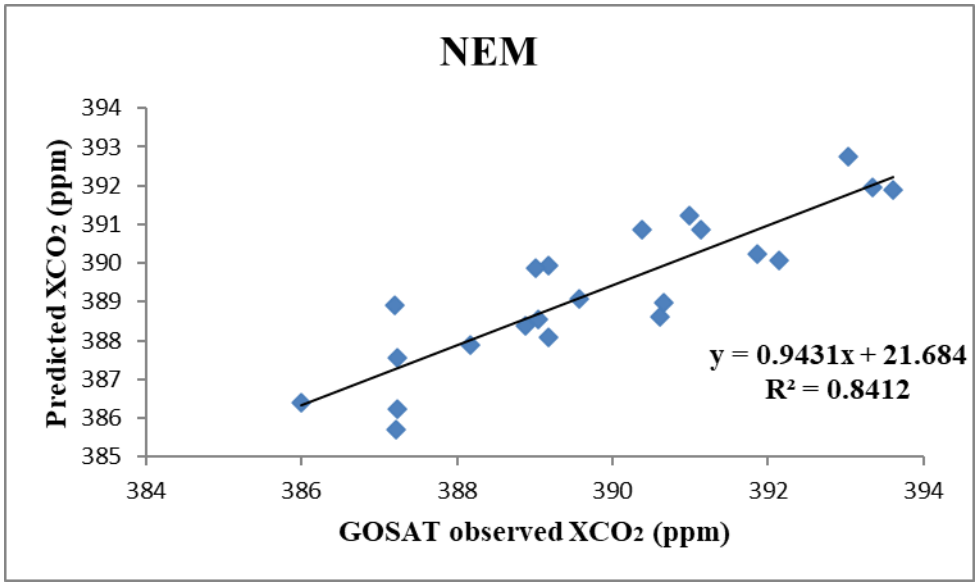

Figure 4. Predicted XCO_2 vs. observed XCO_2 from the GOSAT for the NEM season.

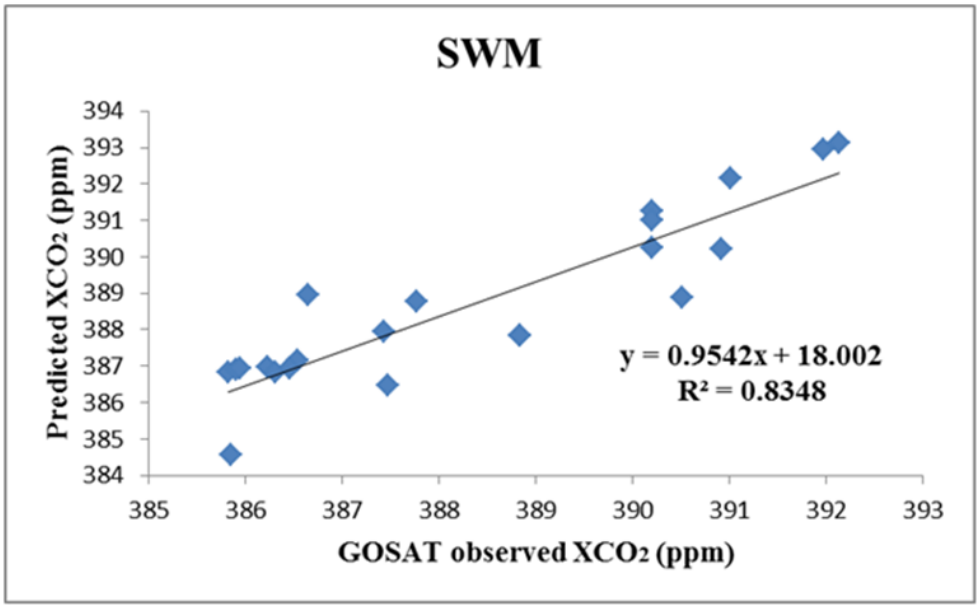

Figure 5. Predicted XCO_2 vs. observed XCO_2 from the GOSAT for the SWM season.

Furthermore, the regression coefficients were statistically significant, and the ρ value of all the coefficients was less than 0.05. The high correlations suggest that the predicted regression model is accurate and efficient. Consequently, all points cluster along the 45° tangent, providing more evidence of model efficiency. Slight discrepancies were found between the predicted XCO_2 and observed XCO_2 values for the AIRS instrument and GOSAT during the NEM and SWM

seasons. These findings may be attributed to factors not considered in this study, including meteorological parameters (wind speed, precipitation, relative humidity and mean surface pressure).

3.3 Evaluating the Impacts of the Monsoon on XCO_2

Seasonal variations result in XCO_2 fluctuations in the NEM and SWM seasons over Peninsular Malaysia. XCO_2 is positively correlated with both the ambient temperature and wind speed. The most prominent winds in Malaysia are from the northeast and the south. Trade winds generally follow the prevailing monsoon flow except when light winds are modified by terrain. Wind strength is greater during the NEM than in the SWM season (Taira et al., 1996). The strong monsoon and the associated movement of the inter-tropical convergence zone (ITCZ) were also examined in this study. The magnitudes of wind and flow patterns at the 1000 mb pressure level in the atmosphere are shown in Figure 6 and Figure 7, respectively. These figures show the mean synoptic charts and the wind vector characteristics for the NEM and SWM seasons from 2009 to 2013, respectively. Vectors show the resultant wind direction, and the vector length indicates the magnitude of the consequent wind. A colour-coded bar in the map indicates the magnitude of wind for a given speed in units of m/s. Contours show the magnitude of the resultant observed wind speed at a contour interval of 3 m/s. The results demonstrate that the wind direction follows the general wind flow patterns indicative of the SWM and NEM seasons.

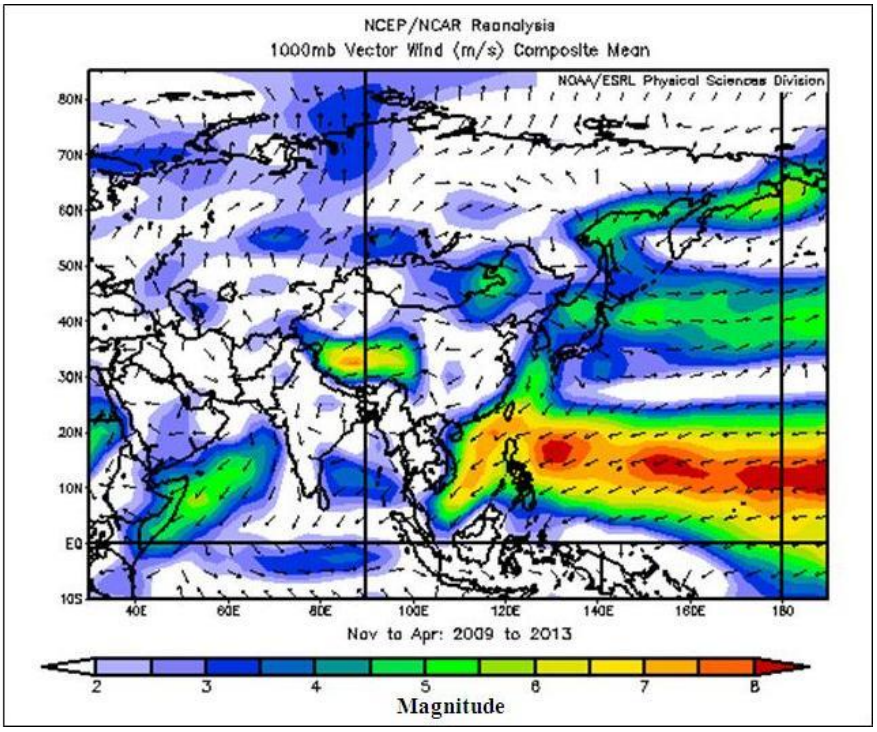

Figure 6. The mean vector wind was 1000 mb over peninsular Malaysia for the NEM from 2009 to 2013.

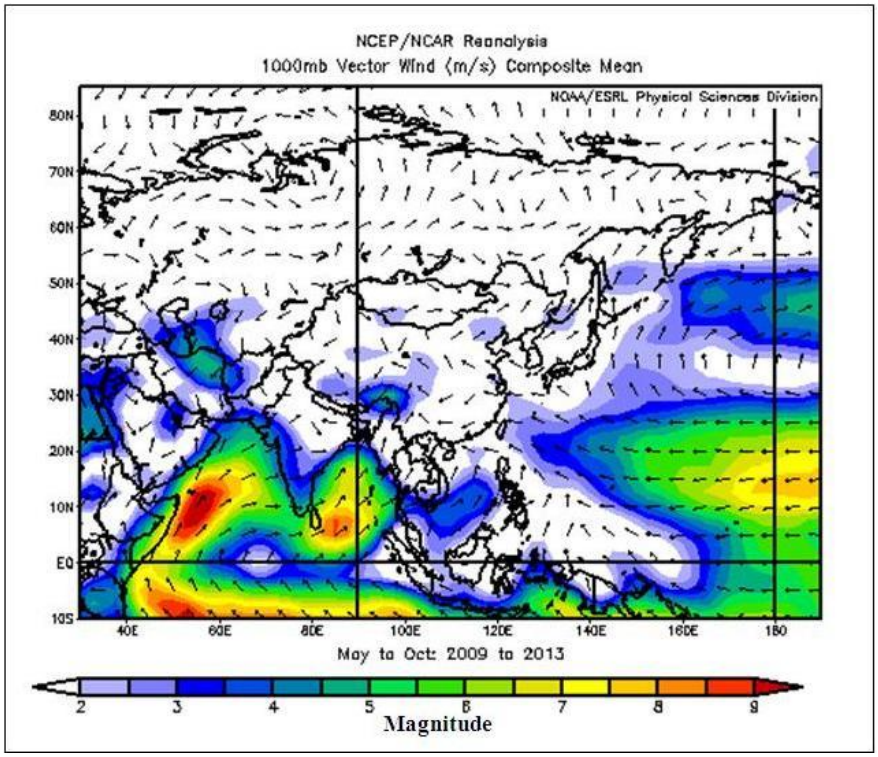

Figure 7. The mean vector wind was 1000 mb over Peninsular Malaysia for the SWM from 2009 to 2013.

The movement and transition of the ITCZ between the two monsoon seasons are distinguishable. When the ITCZ moves southward across Asia and into the Southern Hemisphere, the northeasterly winds transport air masses from the Indian Ocean to peninsular Malaysia during the SWM season (May to October). Subsequently, the ITCZ relocates to the Northern Hemisphere, resulting in long-range transport of air masses from West Asia and the Middle East during the NEM season and a six-month dry period (November to April). Both monsoon seasons are well represented in the mean synoptic charts. Long-range transportation of air pollution was predominantly a result of the outflow from Northeast Asia during the NEM across the Peninsular Malaysia region (see Figure 6). Figure 7 shows the wind vector plots delineating the area of the ITCZ from the data analysis. There is a clear differentiation between the southeast and northeast trade wind systems. Trade wind systems produce an area of strong convergence at the interface from the ITCZ zone associated with the SWM and NEM seasons.

4.0 Conclusion

This paper primarily focuses on developing an algorithm to predict the column-averaged dry air mole fraction of carbon dioxide (XCO_2) over peninsular Malaysia using GOSAT satellite data. Four years of satellite data were employed to develop the algorithms, i.e., XCO_2 in the NEM season and XCO_2 in the SWM season, for calculating XCO_2 over peninsular Malaysia using the MLR method. The best XCO_2 regression equations using MLR for the five independent variables in the NEM and SWM seasons resulted in R^2 values of 0.682 and 0.643, respectively. This result indicates that the atmospheric variables and XCO_2 are highly correlated over the study period. The linear regression correlation validation results were performed for XCO_2 with the observed XCO_2 values from the AIRS instrument and GOSAT satellite. The adjusted coefficients (R^2) of the validation for the NEM and SWM seasons were 0.8412 and 0.8348, respectively. The results revealed that the predicted XCO_2 values were nearly the same as the observed XCO_2 values from AIRS and GOSAT. Further research is required to investigate the effect of radiation on the CO_2 biosphere flux, humidity, rainfall, and wind speed. Finally, air pollution transport to continental Southeast Asia due to the long-range transport of air masses from Northeast and West Asia during the monsoon season should also be examined in future research. As additional satellites for assessing the CO_2 have been premeditated to launch in future, satellite observations of CO_2 should have a

vital application perspective in understanding the variation of global atmospheric CO_2, computing regional CO_2 emission, and integrating the model to evaluate the carbon fluxes.

Acknowledgement

The authors gratefully acknowledge JAXA for providing the GOSAT data used in this paper. This research was supported by the GOSAT project under "The 4th Research Announcement Themes on GOSAT - Regression analysis in modelling of carbon dioxide and factors affecting its value in Peninsular Malaysia". The authors acknowledge the Ministry of Higher Education (MOHE) for funding under the Fundamental Research Grant Scheme (FRGS) (Reference Code: FRGS/1/2021/STG08/USM/02/2).

References

Abdul-Wahab, S. A., Bakheit, C. S., & Al-Alawi, S. M. (2005). Principal component and multiple regression analysis in modelling of ground-level ozone and factors affecting its concentrations. *Environmental Modelling & Software*, *20*(10), 1263-1271.

Ahmad, S., & Yassen, M. E. 2005: Urban climate research in Malaysia. International Association for Urban Climate Newsletter (12, August 2005), 5-10.

Al-Alawi, S. M., Abdul-Wahab, S. A., & Bakheit, C. S. (2008). Combining principal component regression and artificial neural networks for more accurate predictions of ground-level ozone. *Environmental Modelling & Software*, *23*(4), 396-403.

American Meteorological Society. (2012). Climate change: An information statement of the American Meteorological Society. *Bull. Amer. Met. Soc.*

Artuso, F., Chamard, P., Piacentino, S., Sferlazzo, D. M., De Silvestri, L., Di Sarra, A., ... & Monteleone, F. (2009). Influence of transport and trends in atmospheric CO2 at Lampedusa. *Atmospheric Environment*, *43*(19), 3044-3051.

Aumann, H. H., Chahine, M. T., Gautier, C., Goldberg, M. D., Kalnay, E., McMillin, L. M., ... & Susskind, J. (2003). AIRS/AMSU/HSB on the Aqua mission: Design, science objectives, data products, and processing systems. *IEEE Transactions on Geoscience and Remote Sensing*, *41*(2), 253-264.

Azid, A., Juahir, H., Toriman, M. E., Kamarudin, M. K. A., Saudi, A. S. M., Hasnam, C. N. C., ... & Yamin, M. (2014). Prediction of the level of air pollution using principal component

analysis and artificial neural network techniques: A case study in Malaysia. *Water, Air, & Soil Pollution*, *225*, 1-14.

Baker, D. F., Bösch, H., Doney, S. C., O'Brien, D., & Schimel, D. S. (2010). Carbon source/sink information provided by column CO 2 measurements from the Orbiting Carbon Observatory. *Atmospheric Chemistry and Physics*, *10*(9), 4145-4165.

Berger, A. (2000). Global warming, fact or fiction, "From weather forecasting to exploring the solar system". Edited by C Boutron, ERCA Series, Volume 4, Chapter 2, EDP Sciences.

Blunden, J., & Arndt, D. S. (2012). State of the climate in 2011. *Bulletin of the American Meteorological Society*, *93*(7), S1-S282.

Bösch, H., Toon, G. C., Sen, B., Washenfelder, R. A., Wennberg, P. O., Buchwitz, M., ... & Yung, Y. L. (2006). Space-based near-infrared CO2 measurements: Testing the Orbiting Carbon Observatory retrieval algorithm and validation concept using SCIAMACHY observations over Park Falls, Wisconsin. *Journal of Geophysical Research: Atmospheres*, *111*(D23).

Bril, A., Oshchepkov, S., & Yokota, T. (2012). Application of a probability density function-based atmospheric light-scattering correction to carbon dioxide retrievals from GOSAT over-sea observations. *Remote Sensing of Environment*, *117*, 301-306.

Butler, J. H., & Montzka, S. A. (2016). The NOAA annual greenhouse gas index (AGGI). *NOAA Earth System Research Laboratory*, *58*, 55-75.

Chahine, M. T., Chen, L., Dimotakis, P., Jiang, X., Li, Q., Olsen, E. T., ... & Yung, Y. L. (2008). Satellite remote sounding of mid-tropospheric CO2. *Geophysical Research Letters*, *35*(17).

Chahine, M., Barnet, C., Olsen, E. T., Chen, L., & Maddy, E. (2005). On the determination of atmospheric minor gases by the method of vanishing partial derivatives with application to CO2. *Geophysical Research Letters*, *32*(22).

Chédin, A., Serrar, S., Scott, N. A., Crevoisier, C., & Armante, R. (2003). First global measurement of midtropospheric CO2 from NOAA polar satellites: Tropical zone. *Journal of Geophysical Research: Atmospheres*, *108*(D18).

Chevallier, F., Bréon, F. M., & Rayner, P. J. (2007). Contribution of the Orbiting Carbon Observatory to the estimation of CO2 sources and sinks: Theoretical study in a variational data assimilation framework. *Journal of Geophysical Research: Atmospheres*, *112*(D9).

Crevoisier, C., Chédin, A., Matsueda, H., Machida, T., Armante, R., & Scott, N. A. (2009). First year of upper tropospheric integrated content of CO_2 from IASI hyperspectral infrared observations. *Atmospheric Chemistry and Physics*, *9*(14), 4797-4810.

Crevoisier, C., Heilliette, S., Chédin, A., Serrar, S., Armante, R., & Scott, N. A. (2004). Midtropospheric CO2 concentration retrieval from AIRS observations in the tropics. *Geophysical Research Letters*, *31*(17).

Crisp, D., Atlas, R. M., Breon, F. M., Brown, L. R., Burrows, J. P., Ciais, P., ... & Schroll, S. (2004). The orbiting carbon observatory (OCO) mission. *Advances in Space Research*, *34*(4), 700-709.

Cruz, F. T., Narisma, G. T., Villafuerte II, M. Q., Chua, K. C., & Olaguera, L. M. (2013). A climatological analysis of the southwest monsoon rainfall in the Philippines. *Atmospheric Research*, *122*, 609-616.

Dimitriadou, S., & Nikolakopoulos, K. G. (2022). Multiple linear regression models with limited data for the prediction of reference evapotranspiration of the Peloponnese, Greece. *Hydrology*, *9*(7), 124.

Dubovik, O., Holben, B., Eck, T. F., Smirnov, A., Kaufman, Y. J., King, M. D., ... & Slutsker, I. (2002). Variability of absorption and optical properties of key aerosol types observed in worldwide locations. *Journal of the Atmospheric Sciences*, *59*(3), 590-608.

Finlayson-Pitts, B. J., & Pitts Jr, J. N. (1999). *Chemistry of the upper and lower atmosphere: theory, experiments, and applications*. Elsevier.

Haskins, R. D., & Kaplan, L. D. (1993). Remote sensing of trace gases using the atmospheric infrared sounder (AIRS). In *IRS'92: Current Problems in Atmospheric Radiation: Proceedings of the International Radiation Symposium, Tallinn, Estonia, 3-8 August 1992* (p. 278). A. Deepak Publishing.

Hofmann, D. J., Butler, J. H., & Tans, P. P. (2009). A new look at atmospheric carbon dioxide. *Atmospheric Environment*, *43*(12), 2084-2086.

Houghton, R., van der Werf, G., DeFries, R., Hansen, M., House, J., Pongratz, J., & Ramankutty, N. (2012). Regional carbon cycle assessment and processes (RECCAP) synthesis chapter G2: carbon emissions from land use and land-cover change Biogeosci. *Discuss*, *9*, 835-78.

Houweling, S., Breon, F. M., Aben, I., Rödenbeck, C., Gloor, M., Heimann, M., & Ciais, P. (2004). Inverse modeling of CO 2 sources and sinks using satellite data: a synthetic inter-comparison

of measurement techniques and their performance as a function of space and time. *Atmospheric Chemistry and Physics*, *4*(2), 523-538.

Huang, X., Wang, T., Talbot, R., Xie, M., Mao, H., Li, S., ... & Xu, R. (2015). Temporal characteristics of atmospheric CO2 in urban Nanjing, China. *Atmospheric Research*, *153*, 437-450.

Hungershoefer, K., Breon, F. M., Peylin, P., Chevallier, F., Rayner, P., Klonecki, A., ... & Marshall, J. (2010). Evaluation of various observing systems for the global monitoring of CO_2 surface fluxes. *Atmospheric Chemistry and Physics*, *10*(21), 10503-10520.

Huntzinger, D. N., Post, W. M., Wei, Y., Michalak, A. M., West, T. O., Jacobson, A. R., ... & Cook, R. (2012). North American Carbon Program (NACP) regional interim synthesis: Terrestrial biospheric model intercomparison. *Ecological Modelling*, *232*, 144-157.

IPCC. (2013). Summary for Policymakers, In: Climate Change 2013: The Physical Science Basis. Contribution of Working Group I to the Fifth Assessment Report of the Intergovernmental Panel on Climate Change. Cambridge University Press, Cambridge, United Kingdom and New York, USA.

JAXA. (2015). Available online: http://www.jaxa.jp/projects/sat/gosat/index_j.html/ (Accessed on 15 April 2015).

Keat, S. C., Chun, B. B., San, L. H., & Jafri, M. Z. M. (2015, April). Multiple regression analysis in modelling of carbon dioxide emissions by energy consumption use in Malaysia. In *AIP Conference Proceedings* (Vol. 1657, No. 1). AIP Publishing.

Khattak, P., Khokhar, M. F., & Yasmin, N. (2014). Spatio-temporal analyses of atmospheric sulfur dioxide column densities over Pakistan by using SCIAMACHY data. *Aerosol and Air Quality Research*, *14*(7), 1883-1896.

Kim, S. J., Bae, S. J., & Jang, M. W. (2022). Linear regression machine learning algorithms for estimating reference evapotranspiration using limited climate data. *Sustainability*, *14*(18), 11674.

Kim, S. W., Jung, D., & Choung, Y. J. (2020). Development of a multiple linear regression model for meteorological drought index estimation based on Landsat satellite imagery. *Water*, *12*(12), 3393.

Kulawik, S. S., Jones, D. B. A., Nassar, R., Irion, F. W., Worden, J. R., Bowman, K. W., ... & Jacobson, A. R. (2010). Characterization of Tropospheric Emission Spectrometer (TES) CO 2 for carbon cycle science. *Atmospheric Chemistry and Physics*, *10*(12), 5601-5623.

Kuze, A., Suto, H., Nakajima, M., & Hamazaki, T. (2009). Thermal and near infrared sensor for carbon observation Fourier-transform spectrometer on the Greenhouse Gases Observing Satellite for greenhouse gases monitoring. *Applied Optics*, *48*(35), 6716-6733.

Le Marshall, J., Jung, J., Derber, J., Chahine, M., Treadon, R., Lord, S. J., ... & Tahara, Y. (2006). Improving global analysis and forecasting with AIRS. *Bulletin of the American Meteorological Society*, *87*(7), 891-894.

Lindsey, R. (2022). Climate Change: Atmospheric Carbon Dioxide. Available online: https://www.climate.gov/news-features/understanding-climate/climate-change-atmospheric-carbon-dioxide#:~:text=June%2023%2C%202022-,Highlights,2021%3A%20414.72%20parts%20per%20million (Accessed on 24 Dec. 2022).

Mahapatra, A. (2010). Prediction of daily ground-level ozone concentration maxima over New Delhi. *Environmental Monitoring and Assessment*, *170*, 159-170.

Marquis, M., & Tans, P. (2008). Carbon crucible. *Science*, *320*(5875), 460-461.

Miller, C. E., Crisp, D., DeCola, P. L., Olsen, S. C., Randerson, J. T., Michalak, A. M., ... & Law, R. M. (2007). Precision requirements for space-based data. *Journal of Geophysical Research: Atmospheres*, *112*(D10).

Miyamoto, Y., Inoue, M., Morino, I., Uchino, O., Yokota, T., Machida, T., ... & Patra, P. K. (2013). Atmospheric column-averaged mole fractions of carbon dioxide at 53 aircraft measurement sites. *Atmospheric Chemistry and Physics*, *13*(10), 5265-5275.

Morino, I., Uchino, O., Inoue, M., Yoshida, Y., Yokota, T., Wennberg, P. O., ... & Rettinger, M. (2010). Preliminary validation of column-averaged volume mixing ratios of carbon dioxide and methane retrieved from GOSAT short-wavelength infrared spectra. *Atmospheric Measurement Techniques Discussions*, *3*(6), 5613-5643.

NIES GOSAT Project, 2012: Summary of the GOSAT Level 2 Data Products Validation Activity.

Olivier, J. G., Janssens-Maenhout, G., Muntean, M., & Peters, J. A. H. W. (2012). Trends in global CO2 emissions; 2012 Report. PBL Netherlands Environmental Assessment Agency. *Institute for Environment and Sustainability of the European Commission's Joint Research Centre*.

Omar, D. (2009). Urban form and sustainability of a hot humid city of Kuala Lumpur. *European Journal of Social Sciences*, *8*(2), 353-359.

Peters, G. P., Marland, G., Le Quéré, C., Boden, T., Canadell, J. G., & Raupach, M. R. (2012). Rapid growth in CO2 emissions after the 2008–2009 global financial crisis. *Nature Climate Change*, *2*(1), 2-4.

Pochanart, P., Akimoto, H., Kajii, Y., & Sukasem, P. (2003). Carbon monoxide, regional-scale transport, and biomass burning in tropical continental Southeast Asia: Observations in rural Thailand. *Journal of Geophysical Research: Atmospheres*, *108*(D17).

Pochanart, P., Wild, O., & Akimoto, H. (2004). Air pollution import to and export from East Asia. *Air Pollution: Intercontinental Transport of Air Pollution*, 99-130.

Rajab, J. M., MatJafri, M. Z., & Lim, H. S. (2013). Combining multiple regression and principal component analysis for accurate predictions for column ozone in Peninsular Malaysia. *Atmospheric Environment*, *71*, 36-43.

Rayner, P. J., & O'Brien, D. M. (2001). The utility of remotely sensed CO2 concentration data in surface source inversions. *Geophysical Research Letters*, *28*(1), 175-178.

Reuter, M., Bovensmann, H., Buchwitz, M., Burrows, J. P., Connor, B. J., Deutscher, N. M., ... & Wunch, D. (2011). Retrieval of atmospheric CO2 with enhanced accuracy and precision from SCIAMACHY: Validation with FTS measurements and comparison with model results. *Journal of Geophysical Research: Atmospheres*, *116*(D4).

Reuter, M., Buchwitz, M., Schneising, O., Heymann, J., Bovensmann, H., & Burrows, J. P. (2010). A method for improved SCIAMACHY CO 2 retrieval in the presence of optically thin clouds. *Atmospheric Measurement Techniques*, *3*(1), 209-232.

Revadekar, J. V., Varikoden, H., & Ahmed, S. A. (2016). On the relationship between sea surface temperatures, circulation parameters and temperatures over west coast of India. *Science of the Total Environment*, *551*, 175-185.

Schneising, O., Heymann, J., Buchwitz, M., Reuter, M., Bovensmann, H., & Burrows, J. P. (2013). Anthropogenic carbon dioxide source areas observed from space: assessment of regional enhancements and trends. *Atmospheric Chemistry and Physics*, *13*(5), 2445-2454.

Solomon, S. (Ed.). (2007). *Climate Change 2007-The Physical Science Basis: Working Group I Contribution to The Fourth Assessment Report of the IPCC* (Vol. 4). Cambridge University Press.

Stephens, B. B., Gurney, K. R., Tans, P. P., Sweeney, C., Peters, W., Bruhwiler, L., ... & Denning, A. S. (2007). Weak northern and strong tropical land carbon uptake from vertical profiles of atmospheric CO2. *Science*, *316*(5832), 1732-1735.

Tahara, V. M. S. V. S., & Usami, V. M. (2009). FIP's environmentally conscious solutions and GOSAT. *FUJITSU Sci. Tech. J*, *45*(1), 134-140.

Taira, K., Saadon, M. N. B., Kitagawa, S., & Yanagi, T. (1996). Observation of temperature and velocity in the coastal water off Kuala Terengganu, Malaysia. *Journal of Oceanography*, *52*, 251-257.

Tans, P., NOAA/ESRL (www.esrl.noaa.gov/gmd/ccgg/trends/) and Keeling, R., Scripps Institution of Oceanography (scrippsco2.ucsd.edu/). (2014). (ftp://ftp.cmdl.noaa.gov/products/trends/co2/co2_annmean_mlo.txt).

Tiwari, Y. K., Vellore, R. K., Kumar, K. R., van der Schoot, M., & Cho, C. H. (2014). Influence of monsoons on atmospheric CO2 spatial variability and ground-based monitoring over India. *Science of the Total Environment*, *490*, 570-578.

Tsutsumi, Y., Mori, K., Ikegami, M., Tashiro, T., & Tsuboi, K. (2006). Long-term trends of greenhouse gases in regional and background events observed during 1998–2004 at Yonagunijima located to the east of the Asian continent. *Atmospheric Environment*, *40*(30), 5868-5879.

Varikoden, H., Samah, A. A., & Babu, C. A. (2010). Spatial and temporal characteristics of rain intensity in the peninsular Malaysia using TRMM rain rate. *Journal of Hydrology*, *387*(3-4), 312-319.

Wang, T., Shi, J., Jing, Y., Zhao, T., Ji, D., & Xiong, C. (2014). Combining XCO2 measurements derived from SCIAMACHY and GOSAT for potentially generating global CO2 maps with high spatiotemporal resolution. *PLoS One*, *9*(8), e105050.

Wang, Y., Munger, J. W., Xu, S., McElroy, M. B., Hao, J., Nielsen, C. P., & Ma, H. (2010). CO 2 and its correlation with CO at a rural site near Beijing: implications for combustion efficiency in China. *Atmospheric Chemistry and Physics*, *10*(18), 8881-8897.

Wong, C. L., Venneker, R., Uhlenbrook, S., Jamil, A. B. M., & Zhou, Y. (2009). Variability of rainfall in Peninsular Malaysia. *Hydrology and Earth System Sciences Discussions*, *6*(4), 5471-5503.

Wu, J., Guan, D., Yuan, F., Yang, H., Wang, A., & Jin, C. (2012). Evolution of atmospheric carbon dioxide concentration at different temporal scales recorded in a tall forest. *Atmospheric Environment*, *61*, 9-14.

Wunch, D., Toon, G. C., Blavier, J. F. L., Washenfelder, R. A., Notholt, J., Connor, B. J., ... & Wennberg, P. O. (2011). The total carbon column observing network. *Philosophical Transactions of the Royal Society A: Mathematical, Physical and Engineering Sciences*, *369*(1943), 2087-2112.

Wunch, D., Toon, G. C., Wennberg, P. O., Wofsy, S. C., Stephens, B. B., Fischer, M. L., ... & Zondlo, M. A. (2010). Calibration of the Total Carbon Column Observing Network using aircraft profile data. *Atmospheric Measurement Techniques*, *3*(5), 1351-1362.

Wunch, D., Wennberg, P. O., Toon, G. C., Keppel-Aleks, G., & Yavin, Y. G. (2009). Emissions of greenhouse gases from a North American megacity. *Geophysical Research Letters*, *36*(15).

Yang, Z., Toon, G. C., Margolis, J. S., & Wennberg, P. O. (2002). Atmospheric CO2 retrieved from ground-based near IR solar spectra. *Geophysical Research Letters*, *29*(9), 53-1.

Yokomizo, M. (2008). Greenhouse gases observing SATellite (GOSAT) ground systems. *Fujitsu Sci Tech J*, *44*, 410-7.

Yokota, T., Yoshida, Y., Eguchi, N., Ota, Y., Tanaka, T., Watanabe, H., & Maksyutov, S. (2009). Global concentrations of CO2 and CH4 retrieved from GOSAT: First preliminary results. *Sola*, *5*, 160-163.

Yoshida, Y., Ota, Y., Eguchi, N., Kikuchi, N., Nobuta, K., Tran, H., ... & Yokota, T. (2011). Retrieval algorithm for CO 2 and CH 4 column abundances from short-wavelength infrared spectral observations by the Greenhouse gases observing satellite. *Atmospheric Measurement Techniques*, *4*(4), 717-734.

Yue, T. X., Zhao, M. W., & Zhang, X. Y. (2015). A high-accuracy method for filling voids on remotely sensed XCO2 surfaces and its verification. *Journal of Cleaner Production*, *103*, 819-827.

Yuvaraj, R. M. (2020). Extents of predictors for land surface temperature using multiple regression model. *The Scientific World Journal*, *2020*(1), 3958589.